Inorganic Chemistry

Article

pubs.acs.org/IC

Sustainable Synthesis of Niobia Thin Films with Open Mesopore Channels

Kenji Saito,* Yuki Sato, Shohei Okuyama, Kazuki Matsubara, Tatsuto Yui, and Masayuki Yagi

Department of Materials Science and Technology, Faculty of Engineering, Niigata University, 8050 Ikarashi-2, Niigata 950-2181, Japan

Supporting Information

ABSTRACT: The current approaches to electrochemically synthesizing valve metal-derived nanochannel films with longitudinal nanospaces aligned at a right angle to planar substrates rely on highly toxic fluoride compounds and require severe reaction conditions. Herein, we report on a fluoride-free, room-temperature electrochemical synthesis of a genuine mesoporous niobia thin film from the parent metal. The electrochemical reaction is driven by only a 1 V bias with respect to a Pt counter electrode in an aqueous solution. The solution contained an inexpensive, less toxic potassium hydroxide, and the reaction produced favorable byproducts, namely, recyclable $K_8Nb_6O_{19}$ and H_2.

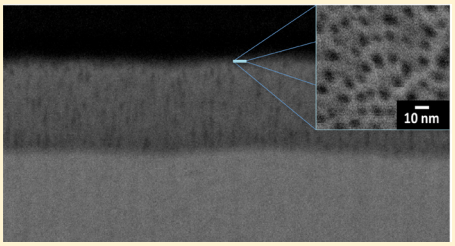

INTRODUCTION

Devising an alternative to the well-established, cost-heavy technology that uses harmful chemicals is a grand challenge imposed on scientists for a sustainable society. In light of increasing amounts of environmental and energy-related issues, current technologies that use nanomaterials for the conversion of solar energy should be further explored. Nb_2O_5 is a recognized simple oxide for solar energy conversion. It is currently used as a cathode substrate in photovoltaic cells, and it is also used as a photocatalyst.[1−5] Nb_2O_5 is well-suited for these roles because the conduction-band minimum (C.B.M) of Nb_2O_5 is higher than that of the more commonly used TiO_2.[6] This boosts the open-circuit voltage in photovoltaic cells, and it increases the driving force of electron transfer from the C.B.M. to the targeted molecules (such as water and organic pollutants in photocatalysis). As substrates for cathodes in photovoltaic cells, current Nb_2O_5 nanomaterials are constructed in a wide variety.[7−9] Among the nanostructures, nanochannel (porous, nanotube, and so forth) films are the most attractive because of the greater contact of ions involved in the photoelectrochemical reaction. Nanochannel films also allow for long-range diffusion of electrons that are produced during photoirradiation. Such favorable phenomena become enhanced when the nanochannels align at right angles to the planar substrate.

Nb_2O_5 films having "open nanochannels" have been synthesized through electrochemical anodization. Generally, the process uses electrolytes that contain toxic fluoride compounds, and the process requires a high bias (~20 V) to drive the anodization.[9−11] However, Schmuki et al.[12] recently reported a fluoride-free route in which a Nb foil is anodized by a 20 V bias in a K_2HPO_4−glycerol mixture at 180 °C. This anodization produced a micrometers thick, porous Nb oxide with contaminants from K_2HPO_4 on its surface. As reported by Habazaki et al.,[13] adding a small amount of water into a similarly mixed system decreases the resultant pore size (from 50 to 10−20 nm). The decreased pore sizes increase the accessible surface area but also lower the apparent structural homogeneity. In addition, removing the contaminants has yet to be addressed.[14]

We report here an unconventional approach to provide a genuine niobia thin film with open mesoporous channels using less-toxic, lower-cost, and recyclable methods (Scheme 1).

Scheme 1. Sustainable Electrochemical Synthesis of Nb_2O_5·nH_2O with Mesoporous Channels[a]

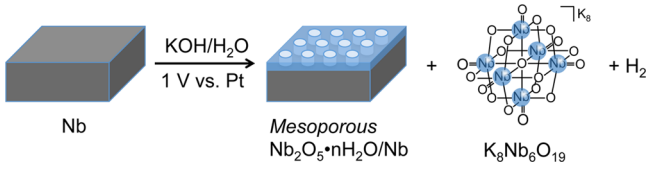

[a]The reaction is driven by a 1 V bias with respect to a Pt counter electrode at room temperature and produces the byproducts $K_8Nb_6O_{19}$ and H_2.

EXPERIMENTAL SECTION

Preparation of Mesoporous Nb_2O_5·nH_2O and Nb_2O_5 Thin Films and a Reference Compound. A 0.1 mm thick Nb foil (The Nilaco Corp., 99.9%) was cleaned chemically. A Nb foil with dimensions of 8 × 33.5 mm was washed with ethanol three times, and it was placed in acetone under ultrasonication for 3 min. The Nb foil was dried under N_2 gas. For the electrochemical anodization, the Nb and Pt (The Nilaco Corp., 99.98%) foils were attached to a 4.5 or 5 mm thick Teflon spacer face to face, and the assembly was soaked in an aqueous KOH solution at 14−20 °C. The immersed dimension was 8 × 11 mm. The constant-potential electrolysis was performed using HZ-7000 (Hokuto Denko) or PA80−1B (TEXIO). The Nb_2O_5·nH_2O

Received: October 24, 2014
Published: February 12, 2015

DOI: 10.1021/ic502580e
Inorg. Chem. 2015, 54, 2171−2175

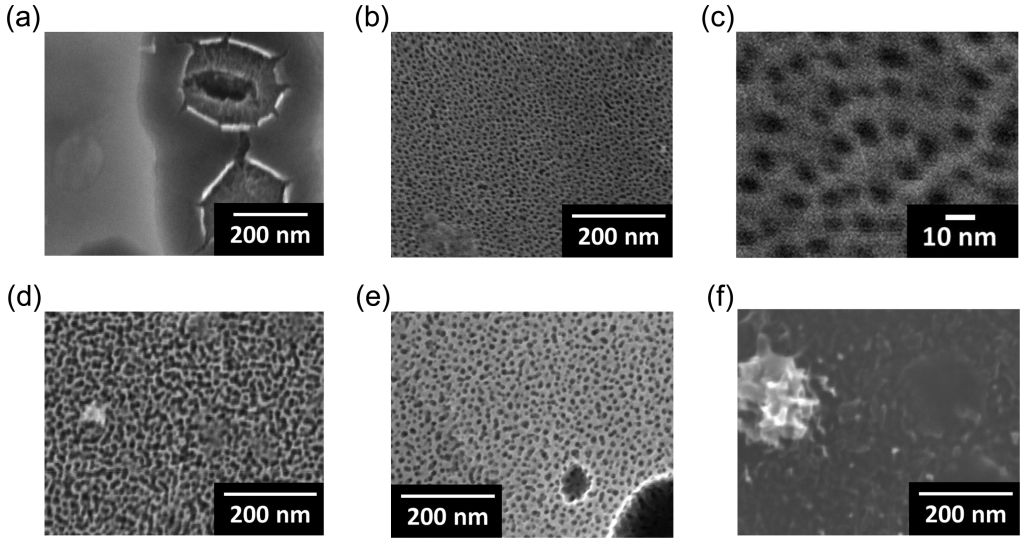

Figure 1. FE-SEM images of 3 h anodized Nb foils under a bias of (a) 0, (b) 1, (d) 2, (e) 5, and (f) 10 V in 1 mol L^{-1} of an aqueous KOH solution stirred at 350 rpm. (c) A magnified view of (b).

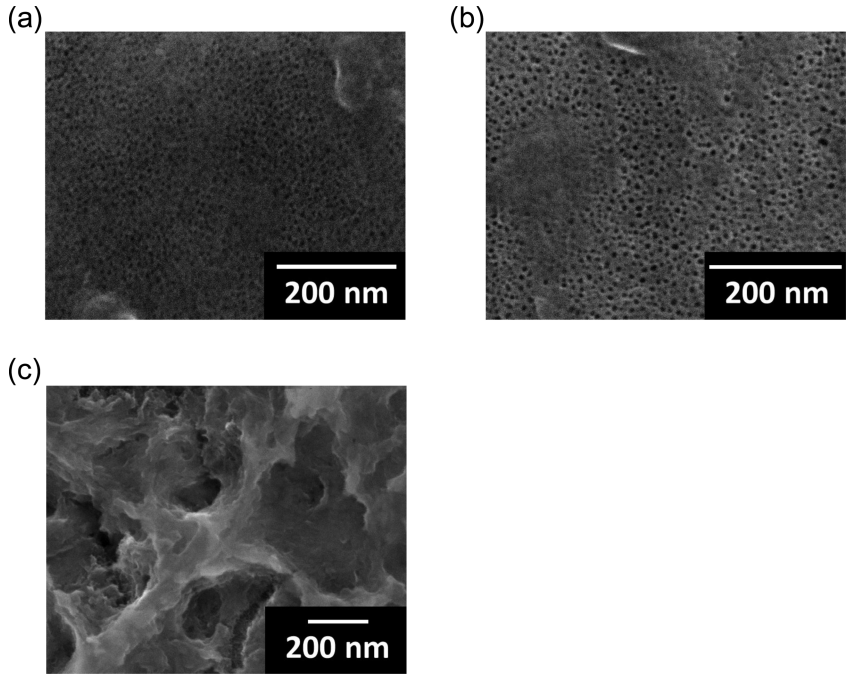

Figure 2. FE-SEM images of 3 h anodized Nb foils under a 1 V bias and stirring rate of 350 rpm in (a) 0.25, (b) 0.5, and (c) 1.5 mol L^{-1} of aqueous KOH solution.

obtained after the electrochemical anodization was crystallized by calcination in air for 1 h at a heating rate of 0.5 °C min^{-1} to afford orthorhombic Nb_2O_5. As a reference, $K_8Nb_6O_{19}$ was prepared according to a previously reported method.[15]

Characterization of the Mesoporous $Nb_2O_5 \cdot nH_2O$ and Nb_2O_5 Thin Films. Field emission scanning electron microscopy (FE-SEM) and the backscattered electron images were taken using JEOL JSM-6500F. The standard deviation in pore size values was estimated from FE-SEM data. X-ray diffraction (XRD) experiments were performed using a Rigaku MiniFlex600 (Cu Kα). Raman spectra were obtained using a LabRAM HR-800 (Horiba). XPS spectra were recorded on JEOL JPS-9000. Focused ion beam (FIB) processing was performed on a HELIOS NANOLAB 650 (FEI), and morphologies were characterized by the SEM. Brunauer–Emmett–Teller (BET) surface areas were measured with a BELSORP-max using krypton (99.995%) as an adsorbing gas. The gas that evolved after the electrochemical synthesis was analyzed by a gas chromatograph (Shimadzu, GC-8APT) equipped with a thermal conductivity detector.

RESULTS AND DISCUSSION

Most reports regarding Nb anodization employ electrolyte solution whose major component is a nonaqueous medium. However, from both environmental and cost-effective viewpoints, water should be the only medium used. $K_8Nb_6O_{19}$ is a water-soluble inorganic crystal. A water-soluble potassium salt such as KOH can stabilize the Nb species that forms during anodization, as $K_8Nb_6O_{19}$ does in water. Additionally, the byproduct can be recycled (for example, as synthetic precursors of coordination compounds and ceramics).[16,17] Thus, KOH was used as an electrolyte in the water. Figure 1 shows the FE-SEM images of Nb foils anodized for 3 h (with [KOH] = 1 mol

DOI: 10.1021/ic502580e
Inorg. Chem. 2015, 54, 2171–2175

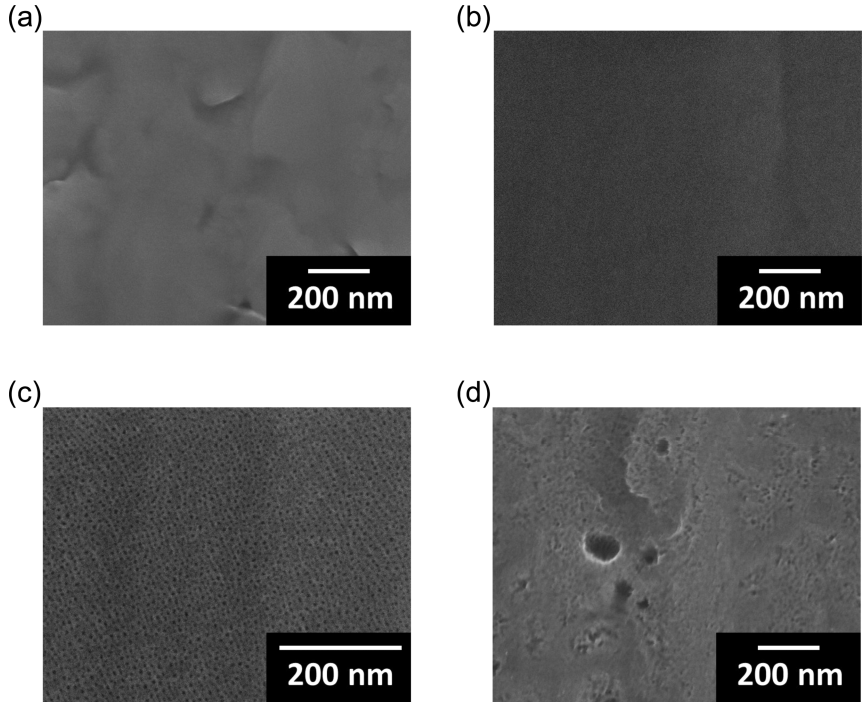

Figure 3. FE-SEM images of 3 h anodized Nb foils with constant bias and rate of stirring (1 V and 350 rpm, respectively) in 1 mol L^{-1} of aqueous solutions containing (a) KH_2PO_4, (b) KNO_3, (c) K_2CO_3, and (d) NaOH electrolytes.

L^{-1} and at a stir rate of 350 rpm). Without applying a bias, 200 nm wide pores were formed from embrittlement by corrosion. Organized nanochannels with diameters of 6 ± 0.9 nm began to appear at a 1 V bias, and increasing the bias by 5 V caused the formation of interconnecting pores. At a 10 V bias, however, rough surfaces with blurred scars were formed. Likewise, the prolonged, 5 h anodization at a 1 V bias exfoliated the nanostructure, resulting in a similar roughened surface. Thus, the rough surface observed at 10 V bias originated from increased rate of anodization and/or the production of H_2/O_2 bubbles (produced from the competing electrolysis of water). We then examined how the concentration of KOH impacts the morphology of the resulting structure (Figure 2). The lowest concentration of KOH (0.25 mol L^{-1}) resulted in pores with diameters less than 5 nm throughout the substrate. Increasing the concentration of KOH increases the size of the pores (Figure 2b), and homogeneous nanostructures with pores 6 ± 0.9 nm in diameter are formed when the concentration of KOH reaches 1 mol L^{-1} (Figure 1b,c). Rough surfaces are formed when concentrations of KOH greater than 1.5 mol L^{-1} are used. These surfaces formed because of the increased rate of anodization at these higher concentrations (Figure 2c). In general, the rate of stirring (which controls mass transport) during the electrochemical synthesis impacts the resultant structure (Supporting Information, Figure S1).[18] Among the stir rates investigated, homogeneous mesopores were visible only at the highest speed (350 rpm). Higher speeds were not investigated because 350 rpm was the maximum rotational speed of the stir bar. This notable dependence has not been observed for the prevailing fluoride systems,[18] and its existence here suggests a different liquid-phase product is formed by the electrochemical reaction. To scrutinize the effect of the counteranions and pH on the structure of the product, additional control experiments were performed at a constant solution concentration (1 mol L^{-1}) but with broader pH ranges (Figure 3 and Supporting Information, Table S1). Potassium salts with $H_2PO_4^-$ and NO_3^- counteranions did not produce any mesoporous structures (neither did strongly alkaline sodium salts such as NaOH). The carbonate salt K_2CO_3, however, produced homogeneous mesopores, but the mean pore diameter was small (4 ± 0.6 nm). A $[K_2CO_3]$ = 1 mol L^{-1} has a slightly basic pH as shown in Table S1.

The mesoporous film was obtained using a 1 V bias with [KOH] = 1 mol L^{-1}. The anodization reaction was stirred at 350 rpm and allowed to run for 3 h. The resulting product had no diffraction peak in the X-ray diffraction (XRD) spectrum. This finding indicates that the as-prepared film after the anodization is amorphous as specified in the reports on the K_2HPO_4–glycerol systems.[12,13] The Raman spectrum, by contrast, exhibits two distinct peaks that correspond to the symmetric stretching modes of the distributed NbO_6, NbO_7, and NbO_8 polyhedra (654 cm^{-1}) and Nb═O (~856 cm^{-1}) of niobic acid ($Nb_2O_5{\cdot}nH_2O$) (Supporting Information, Figure S2).[19] As shown in Supporting Information, Figure S3, the XPS analyses indicated that the phase-pure $Nb_2O_5{\cdot}nH_2O$ thin film does not contain any potassium ions (as might be predicted from using a KOH electrolyte). Cross-sectional images of the mesoporous $Nb_2O_5{\cdot}nH_2O$ were then analyzed to estimate the structure's surface area and apparent growth rate during the anodization. The as-prepared, anodized film has a rough side structure, which prevented accurate microstructural observations using either the secondary electron or backscattered electron detectors equipped with the FE-SEM. To address this difficulty, we employed an FIB technology rather than mechanical cutting, for example, by scissors. This is because cutting applies mechanical pressure, which can cause severe structural damage. FIB, however, sputters material by a convergent beam of Ga ions to expose the inner structure. This process minimally impacts the structure. The resulting image of the FIB processing of the mesoporous $Nb_2O_5{\cdot}nH_2O$ is

DOI: 10.1021/ic502580e
Inorg. Chem. 2015, 54, 2171−2175

shown in Figure 4. As observed, cylindrical mesospaces are aligned at right angles with respect to the planar Nb substrate.

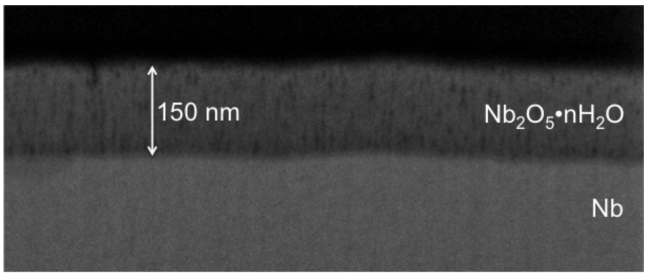

Figure 4. A cross-sectional SEM image of FIB-processed, mesoporous $Nb_2O_5{\cdot}nH_2O$ film.

The $Nb_2O_5{\cdot}nH_2O$ segment has a thickness of 150 nm. Because the anodization time is 3 h, an apparent growth rate of $Nb_2O_5{\cdot}nH_2O$ is estimated to be 0.8 nm min^{-1}, and the rate is slightly slow compared to the rate in the aqueous system containing HF and NaH_2PO_4 (1.0 nm min^{-1}).[20] A net BET surface area of $Nb_2O_5{\cdot}nH_2O$ was calculated to be 575 m^2 cm^{-3}. The calculations were performed as follows: the BET surface area of the films was determined by the krypton adsorption isotherm to be 0.184 m^2 g^{-1}, and the area was divided by a net cubic volume of 3.2×10^{-4} cm^3. The net cubic volume was calculated by multiplying the surface area of the films (21.5 cm^2) by the net film thickness (1.5×10^{-5} cm).

For the electrochemical synthesis of the nanochannel films, a chronoamperometry experiment provides valuable insights into growth mechanisms. The reaction time versus current density characteristics shown in Figure 5 begin with a decrease in the

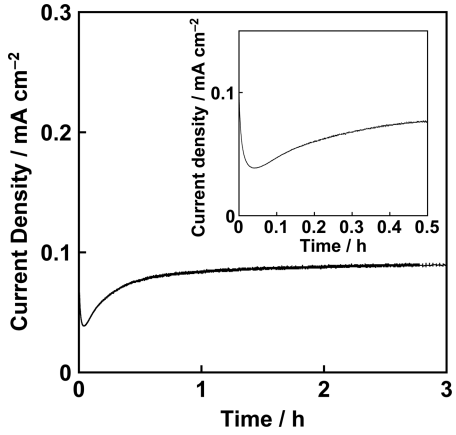

Figure 5. Time-current characteristics for the 3 h anodization in 1 mol L^{-1} of aqueous KOH solution under a constant bias and rate of stirring (1 V and 350 rpm, respectively). (inset) The beginning of the anodization.

current density. Eventually, the current increases sharply and plateaus. This trend is identical to that of well-recognized fluoride systems,[18] and it is thought to occur as a consequence of the following chemical reactions: (1) the initial decrease in the current occurs because niobium oxide forms as a thin layer on the Nb foil and acts as a barrier layer, (2) the niobium oxide starts to dissolve in the solvent as a complex or the other chemical forms, randomly forming pits, and the pit-size-dependent etching process accelerates the dissolution reaction because of the increased surface area, (3) the rates of oxidation and dissolution reactions counterbalance, and the current plateaus. Identifying the byproducts of the reaction will further reinforce the validity of the proposed mechanism, and we first examined the solution-phase products. Even the concentrated solution (produced by evaporating the reaction solution after a 24 h anodization) exhibited very weak Raman scattering. As a result, a crystal was separated from the solution. The visible peaks agreed with the niobium−oxygen vibrations of $K_8Nb_6O_{19}$ (Figure 6). Thus, KOH was confirmed to dissolve the niobium

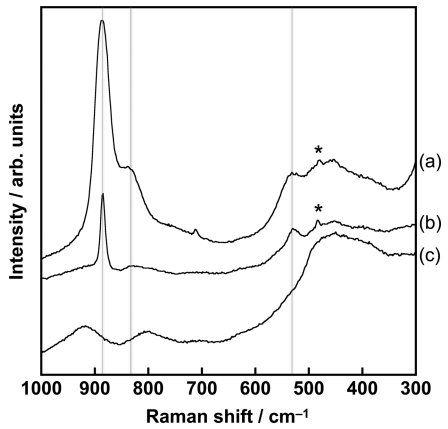

Figure 6. Raman spectra of (a) the reference $K_8Nb_6O_{19}$ crystal in solution, (b) a crystal separated from a concentrated solution after 24 h anodization, and (c) 1 mol L^{-1} of an aqueous KOH solution. Light-colored lines show positions at which characteristic vibrations appear as follows: ν_s(Nb−O−Nb) = 531 cm^{-1}, ν_{antis}(Nb═O) = 831 cm^{-1}, and ν(Nb═O) = 885 cm^{-1}. The subscript words, s and antis, mean symmetric and antisymmetric vibrations, respectively. Asterisks show unknown peaks.

oxide formed during the anodization, forming $K_8Nb_6O_{19}$ as a byproduct in solution. A gas-phase product from a Pt counter electrode was examined as well. N_2-filled electrolysis under the optimized conditions did not afford the targeted mesoporous structure, implying that molecular oxygen is consumed as an oxygen source of $Nb_2O_5{\cdot}nH_2O$. We thus employed a two-compartment cell in which one side with Nb foil is aerated and the other side with Pt is filled with Ar. The 3 h anodization afforded the mesoporous $Nb_2O_5{\cdot}nH_2O$ and H_2, and the Faradaic efficiency for H_2 evolution was estimated to be 94%.

In solution, $K_8Nb_6O_{19}$ exists as a cluster[19,21] with a molecular size much larger than that of the proposed mononuclear fluoride complexes.[18] Considering the Stokes−Einstein theory, $K_8Nb_6O_{19}$ diffuses more slowly than does the fluoride complex in solution. Such a slow diffusion will slow the etching reaction and lead to excessive dependence on the stir rate during anodization. Likewise, even under the conditions in which the mesoporous structure forms, the difference in diffusion rates of the byproducts is thought to impact the growth rate of the niobium oxide. Additionally, the chemical species varies with solution pH, indicating a dependence on the electrolytes. $Nb_6O_{19}^{8-}$ is reported to exist as the predominant species in a strongly alkaline solution (pH = 14.5), and this is consistent with our results (see the Raman spectrum in Figure 6).[22] As the solution pH decreases, the protonated species $H_xNb_6O_{19}^{(8-x)-}$ (x = 1−3) starts to become dominant. At a pH of 8.5 or less, $H_xNb_6O_{19}^{(8-x)-}$ complexes tend to combine with each other to form more complicated structures.[21] An aqueous K_2CO_3 solution (pH = 11.1) affords smaller mesopores, and this

DOI: 10.1021/ic502580e
Inorg. Chem. 2015, 54, 2171−2175

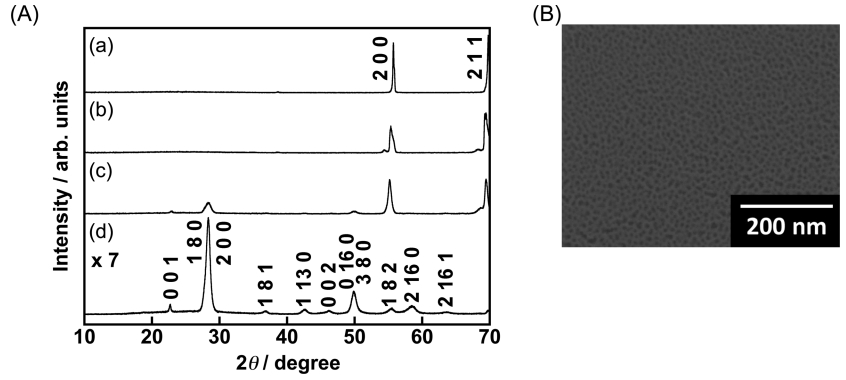

Figure 7. (A) XRD patterns of (a) the unprocessed Nb foil and anodized samples calcined at (b) 350, (c) 400, and (d) 450 °C. The *y*-axis of (d) was enlarged 7 times to specify indexed peaks. (B) FE-SEM image of (d).

finding suggests that $H_xNb_6O_{19}^{(8-x)-}$ hinders the formation of the mesopores. The blocking effect will become pronounced when the polymerized species forms at pH values below 8.5. Using NaOH as an electrolyte does not promote mesopore formation, though the aqueous solution does show a basic pH. This finding is indicated by the absence of the sodium salt of $Nb_6O_{19}^{8-}$.

Calcination at varied temperatures in air was performed to determine the lowest crystallization temperature (Figure 7A). The crystallization into orthorhombic Nb_2O_5[9,14] appears to occur at 400 °C; however, a 450 °C calcination is needed to yield phase-pure Nb_2O_5. The highest calcination temperature had no discernible impact on the local nanostructure, as revealed by the front and cross-sectional FE-SEM images (Figure 7B and Supporting Information, Figure S4).

CONCLUSION

Investigation of the water-soluble inorganic crystal $K_8Nb_6O_{19}$ revealed mechanistic insight into a sustainable electrochemical approach to generate a mesoporous niobia thin film with open mesoporous channels. We examined the critical factors in the growth of the ordered mesopores, and we found that (1) a KOH concentration exceeding 1 mol L^{-1} and a bias greater than 5 V leads to an excessive increase in anodization rate (or formation of H_2/O_2 bubbles in the latter case), hampering the formation of the mesopores, (2) targeted mesopores are visible only at a stir rate of 350 rpm because the byproduct, the $K_8Nb_6O_{19}$ cluster, will diffuse more slowly than does the prevailing mononuclear fluoride complex, and (3) a potassium-based electrolyte and high solution pH are needed to stabilize the discharged Nb species ($K_8Nb_6O_{19}$). The resultant impurity-free nanocrystal thin film is thought to have applications in solar energy conversion; research into this topic is currently underway.

ASSOCIATED CONTENT

Supporting Information

FE-SEM images of films anodized under varied rates of stirring, tabulated electrolyte data, Raman and XPS spectra of an anodized film, and a cross-sectional SEM image of a crystallized film. This material is available free of charge via the Internet at http://pubs.acs.org.

AUTHOR INFORMATION

Corresponding Author

*E-mail: ksaito@eng.niigata-u.ac.jp.

Funding

K.S. acknowledges the financial support of a Grant-in-Aid for Young Scientists B (No. 26790012) from the Ministry of Education, Culture, Sports, Science and Technology (MEXT) of Japan, the Kurata Memorial Hitachi Science and Technology Foundation, and the Uchida Energy Science Foundation.

Notes

The authors declare no competing financial interest.

REFERENCES

(1) Grätzel, M. *J. Photochem. Photobiol. C* **2003**, *4*, 145−153.
(2) Hafeldt, A.; Boschloo, G.; Sun, L.; Kloo, L.; Pettersson, H. *Chem. Rev.* **2010**, *110*, 6595−6663.
(3) Rühle, S.; Shalom, M.; Zaban, A. *ChemPhysChem* **2010**, *11*, 2290−2304.
(4) Ge, S.; Jia, H.; Zhao, H.; Zheng, Z.; Zhang, L. *J. Mater. Chem.* **2010**, *20*, 3052−3058.
(5) Lang, X.; Chen, X.; Zhao, J. *Chem. Soc. Rev.* **2014**, *43*, 473−486.
(6) Lenzmann, F.; Krueger, J.; Burnside, S.; Brooks, K.; Grätzel, M.; Gal, D.; Rühle, S.; Cahen, D. *J. Phys. Chem. B* **2001**, *105*, 6347−6352.
(7) Viet, A. L.; Jose, R.; Reddy, M. V.; Chowdari, B. V. R.; Ramakrishna, S. *J. Phys. Chem. C* **2010**, *114*, 21795−21800.
(8) Kim, H.-N.; Moon, J. H. *ACS Appl. Mater. Interfaces* **2012**, *4*, 5821−5825.
(9) Ou, J. Z.; Rani, R. A.; Ham, M.-H.; Field, M. R.; Zhang, Y.; Zheng, H.; Reece, P.; Zhuiykov, S.; Sriram, S.; Bhaskaran, M.; Kaner, R. B.; Kalantar-zadeh, K. *ACS Nano* **2012**, *6*, 4045−4053.
(10) Choi, J.; Lim, J. H.; Lee, S. C.; Chang, J. H.; Ja Kim, C. K.; Cho, M. A. *Electrochim. Acta* **2006**, *51*, 5502−5507.
(11) Wei, W.; Lee, K.; Shaw, S.; Schmuki, P. *Chem. Commun.* **2012**, *48*, 4244−4246.
(12) Lee, K.; Yang, Y.; Yang, M.; Schmuki, P. *Chem.—Eur. J.* **2012**, *18*, 9521−9524.
(13) Habazaki, H.; Oikawa, Y.; Fushimi, K.; Aoki, Y.; Shimizu, K.; Skeldon, P.; Thompson, G. E. *Electrochim. Acta* **2009**, *54*, 946−951.
(14) Rani, R. A.; Zoolfakar, A. S.; Ou, J. Z.; Ab. Kadir, R.; Nili, H.; Latham, K.; Sriram, S.; Bhaskaran, M.; Zhuiykov, S.; Kaner, R. B.; Kalantar-zadeh, K. *Chem. Commun.* **2013**, *49*, 6349−6351.
(15) Saito, K.; Kudo, A. *Bull. Chem. Soc. Jpn.* **2009**, *82*, 1030−1034.
(16) Saito, K.; Kudo, A. *Inorg. Chem.* **2010**, *49*, 2017−2019.
(17) Nyman, M.; Rodriguez, M. A.; Alam, T. M.; Anderson, T. M.; Ambrosini, A. *Chem. Mater.* **2009**, *21*, 2201−2208.
(18) Moseke, C.; Lehmann, C.; Schmitz, T.; Reinert, F.; Groll, J.; Gbureck, U. *Current Nanosci.* **2013**, *9*, 132−138.
(19) Pugh, C.; Percec, V. *Chem. Mater.* **1991**, *3*, 107−115.
(20) Saule, A. G.; Aldabergenova, S.; Tsuchyia, H.; Schmuki, P. *Angew. Chem., Int. Ed.* **2006**, *45*, 6993−6996.
(21) Black, J. R.; Nyman, M.; Casey, W. H. *J. Am. Chem. Soc.* **2006**, *128*, 14712−14720.
(22) Jehng, J.-M.; Wachs, I. E. *J. Raman Spectrosc.* **1991**, *22*, 83−89.

DOI: 10.1021/ic502580e
Inorg. Chem. 2015, 54, 2171−2175